FUNCTIONAL
MATERIALS

Effect of Pb(Zn$_{1/3}$Nb$_{2/3}$)O$_3$ addition on structural, dielectric, Raman, and ferroelectric properties of BaTiO$_3$ ceramics

Jan Suchanicz[a*], Halina Czternastek[b], Kamila Kluczewska[a], Piotr Czaja[a], Adrian Węgrzyn[a], Mariusz Sokolowski[c], Erazm Maria Dutkiewicz[d], and Jerzy Szczęsny[e]

[a] Institute of Technics, Pedagogical University, ul. Podchorazych 2, 30-084 Krakow, Poland
[b] Institute of Physics, Pedagogical University, ul. Podchorazych 2, 30-084 Krakow, Poland
[c] Faculty of Computer Science, Electronics and Telecommunications, AGH University of Science &Technology, ave. Mickiewicza 30, 30-059 Krakow, Poland
[d] Institute of Nuclear Physics PAN, ul. Radzikowskiego 152, 31-342 Krakow, Poland
[e] Institute of Computer Science, Pedagogical University, ul. Podchorazych 2, 30-084 Krakow, Poland

Abstract. A $(1-x)$BaTiO$_3$–xPb(Zn$_{1/3}$Nb$_{2/3}$)O$_3$ $((1-x)$BT–xPZN) system with a low content of PZN ($x = 0$, 0.025, and 0.05) was prepared by the spark plasma sintering process. X-ray diffraction analysis exhibited that the obtained specimens possessed the perovskite structure with tetragonal symmetry and underwent a sequence of phase transformations characteristic of pure BT. The microstructure study showed a dense structure in good agreement with that of above 95% relative density determined by the Archimedes method. Dielectric measurements revealed that the maximum of electric permittivity was broadened and shifted after the PZN doping of BT. The Raman spectra were similar for all samples in agreement with the X-ray data. It was shown that the PZN doping of BT caused a worsening of ferroelectric properties. The obtained results are discussed in terms of an increased degree of crystal structure disorder, which creates local elastic and electric fields. The investigated ceramics are considered to be a good starting point for low-lead electronic materials.

Key words: perovskite, ferroelectric materials, dielectric spectroscopy.

1. INTRODUCTION

Lead-based ceramic materials are the most widely used piezoelectric materials due to their excellent dielectric and piezoelectric properties [1,2]. However, environmental and health concerns regarding the toxicity of lead have caused restrictions on their use in electronic devices. Therefore, a number of lead-free or low-lead-content materials have been studied with the aim of replacing lead-containing materials. With this point of view, $(1-x)$BaTiO$_3$–xPb(Zn$_{1/3}$Nb$_{2/3}$)O$_3$ $((1-x)$BT–xPZN) ceramics with a low content of PZN ($x = 0$, 0.025, and 0.05) were prepared by the Spark Plasma Sintering (SPS) process, and their structural, dielectric, Raman, and ferroelectric properties were investigated.

2. EXPERIMENTAL CONDITIONS

In the first stage good quality BT–PZN ceramics were attempted to be obtained by the conventional sintering method. Unfortunately, the samples obtained in this way were rather fragile, with their density below 88% of the theoretical value, and they displayed low resistivity. Therefore, the next samples were obtained by a SPS route.

___
[*] Corresponding author, sfsuchan@gmail.com

The materials were sintered using the SPS equipment (FCT system, Germany). The powders (without a plasticizer) of basic oxides $BaCO_3$, TiO_2, Nb_2O_5, PbO, and ZnO were placed in a graphite die (inner diameter of 20 mm) and uniaxially pressed at 35 MPa. They were then heated up to 1190 °C with a heating rate of 100 °C/min and sintered at the final temperature for 5 min. After the sintering process, the samples were first allowed to cool within the matrix and then removed. The entire SPS process took place in the protective Ar atmosphere. After SPS sintering, the sample was annealed in air at 1000 °C for 2 h to remove the carbon contamination. The obtained samples reveal a pure perovskite phase with a relative density above 96%.

Structural tests were performed by an X-ray diffraction (XRD) method. Measurements of the synthesized materials were taken using a Panalytical Empyrean diffractometer in a 10–110° range with CuK_α radiation. For high-temperature measurements (from 30 to 300 °C), the diffractometer was equipped with an Anton Paar HTK 1200N oven chamber. In the low temperature range (–250 to 20 °C), an Oxford cryostat was mounted and evacuated by using rotary and turbomolecular pumps. Rietveld analysis of the XRD data was supported by GSAS/EXPGUI software. For clarity, the results shown in the respective figures were numerically stripped of the $K_{\alpha 2}$ component by the Rachinger method.

The microstructure of the synthesized ceramics was analysed using a Model Hitachi S4700 scanning microscope (SEM) with field emission and the Noran Vantage EDS system.

The specific heat measurements were taken with a Netzsch DSC F3 Maia scanning calorimeter (DSC) over the temperature range from –150 to 300 °C under an argon atmosphere, at a flow rate of 30 mL/min. The specimen consisting of a single piece of material with an average mass of 20 mg was placed in an alumina crucible. Measurement data were collected upon heating and cooling with a constant rate of 10 °C/min.

Raman spectra were recorded with a Bio-Rad FTS 6000 spectrometer with an Nd:Yag laser system, where the 1064 nm line was used as the excitation line. The laser power was 200 mW, and the spectra were collected with 4 cm^{-1} resolution.

The dielectric measurements were taken for silver electrode samples using a GW 821 LCR meter over the temperature/frequency range from –75 to 300 °C and from 20 to 2 MHz, respectively, and under the applied electric field of 20 V/cm. The data were collected with a step of 0.1 °C upon heating and cooling, with the temperature variation at a rate of 100 °C/h and by using an automatic temperature controller.

The polarization versus electric field (P–E) hysteresis loops were obtained at 50 Hz with the aid of a Sawyer–Tower circuit.

3. RESULTS AND DISCUSSION

Figure 1 shows SEM micrographs of (1-*x*)BT–*x*PZN ceramics. Well-developed grains with grain size about 6 mm for BT and about 0.4–0.5 μm for BT–PZN were observed.

Figure 2 shows XRD patterns of investigated ceramics as a function of temperature. As can be seen, all ceramics exhibit a tetragonal single-phase perovskite-type crystal structure (space group 4 mm) at room temperature. Compared to the pure BT, the recorded structural transformations of 0.975BT–0.025PZN and 0.95BT–0.05PZN are not well defined revealing broader peaks due to the increasing disorder of the crystal structure. In addition, no significant changes in temperatures of phase transitions can be noticed. Also the transformations temperatures cannot be accurately determined because of the presence of relatively broad peaks. Generally, PZN doping affects BT differently than PMN [3–5]; PMN causes cubic phase to stable down to lower temperature.

Dielectric measurements reveal that BT–PZN ceramics underwent a sequence of phase transformations similar to undoped BT (Fig. 3), in accordance with XRD results. The dielectric permittivity ε(*T*) peaks shift towards the higher temperature for 0.975BT–0.025PZN and towards the lower temperature for 0.95BT–0.05PZN. The ε(*T*) peaks become broader and dielectric dispersion increases after PZN incorporation into BT.

The DSC curves for pure BT reveal three anomalies attributed to phase transformations (Fig. 4). The anomalies become smaller and broader after PZN incorporation into BT. In addition, these anomalies shift irregularly with temperature.

The broadening of the XRD, DSC, and ε(*T*) peaks is related to an increase of the degree of A- and B-site disorder due to the presence of Pb^{2+} and $(Zn,Nb)^{4+}$ ions.
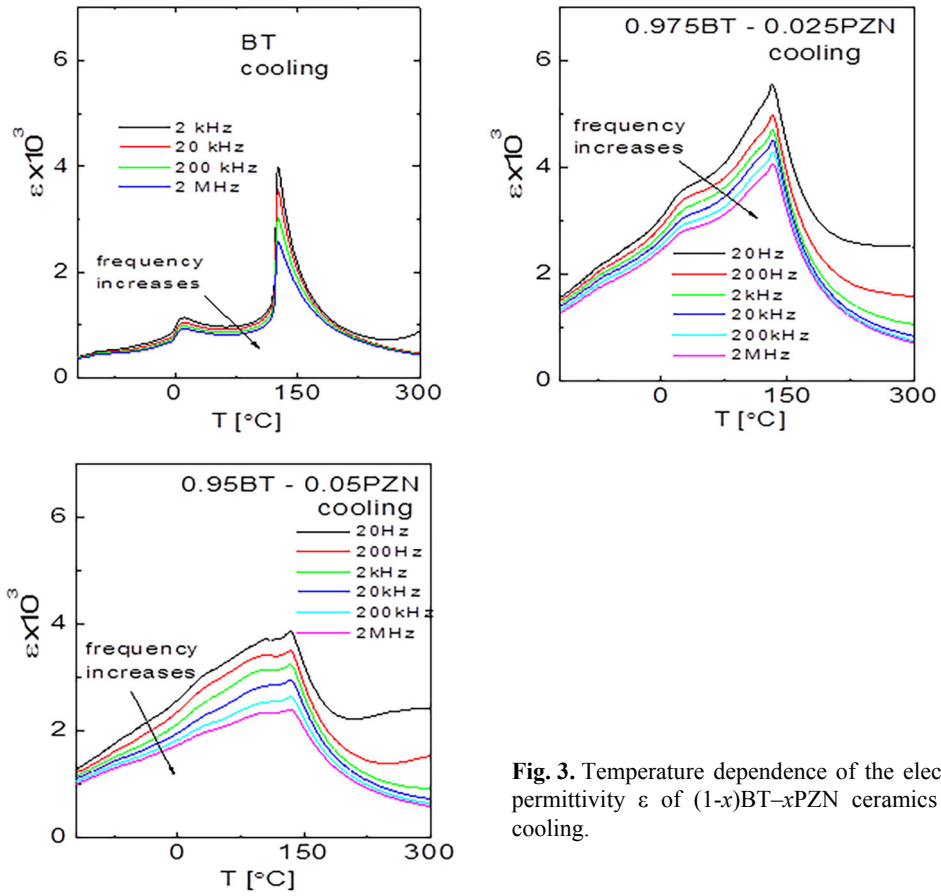
Room-temperature Raman spectra of BT and BT–PZN are shown in Fig. 5. A sharp peak near 310 cm^{-1} and a broad peak near 720 cm^{-1} for pure BT are characteristic of the tetragonal phase. Generally 180 cm^{-1}, 310 cm^{-1}, and 720 cm^{-1} bands are regarded as the signature of the ferroelectric phase in BT. Thus, it is evident from Fig. 5 that BT is in its tetragonal ferroelectric phase. The high-frequency bonds above 700 cm^{-1} are related to the existence of oxygen vibrations and oxygen vacancies [5]. Similar Raman spectra of BT ceramics were reported by Farhi et al. [6]. The Raman spectra of BT and BT–PZN are similar to each other.
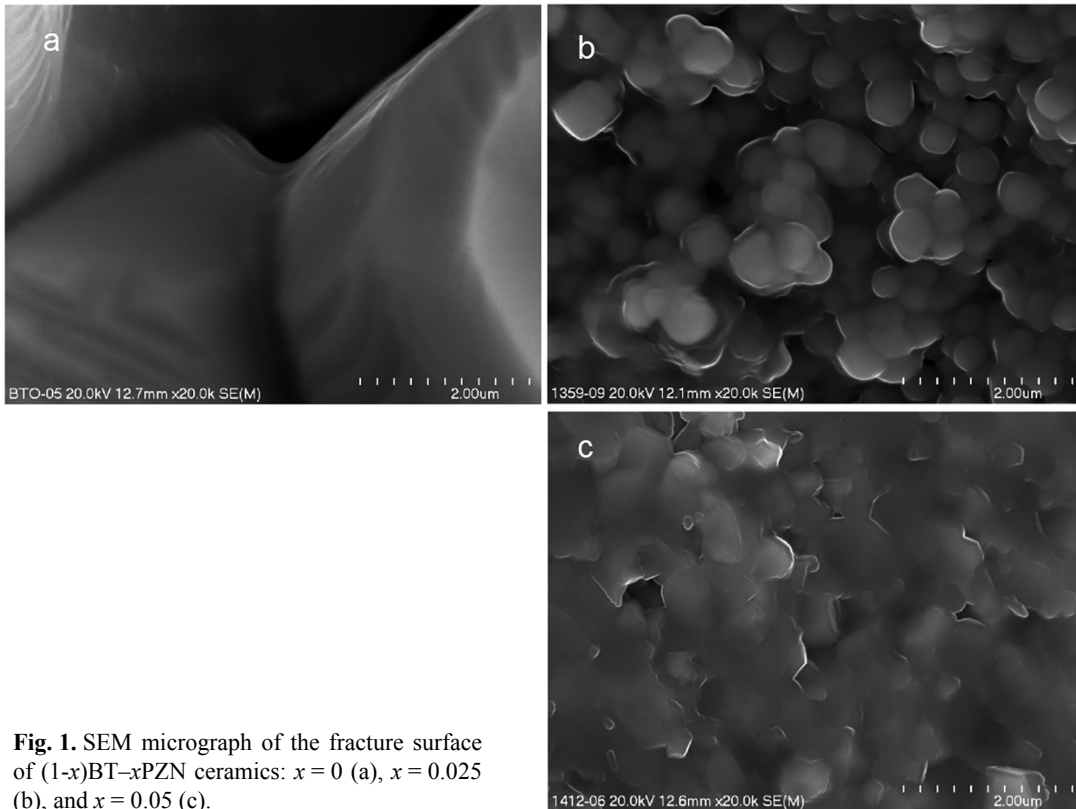
Fig. 1. SEM micrograph of the fracture surface of (1-x)BT–xPZN ceramics: $x = 0$ (a), $x = 0.025$ (b), and $x = 0.05$ (c).
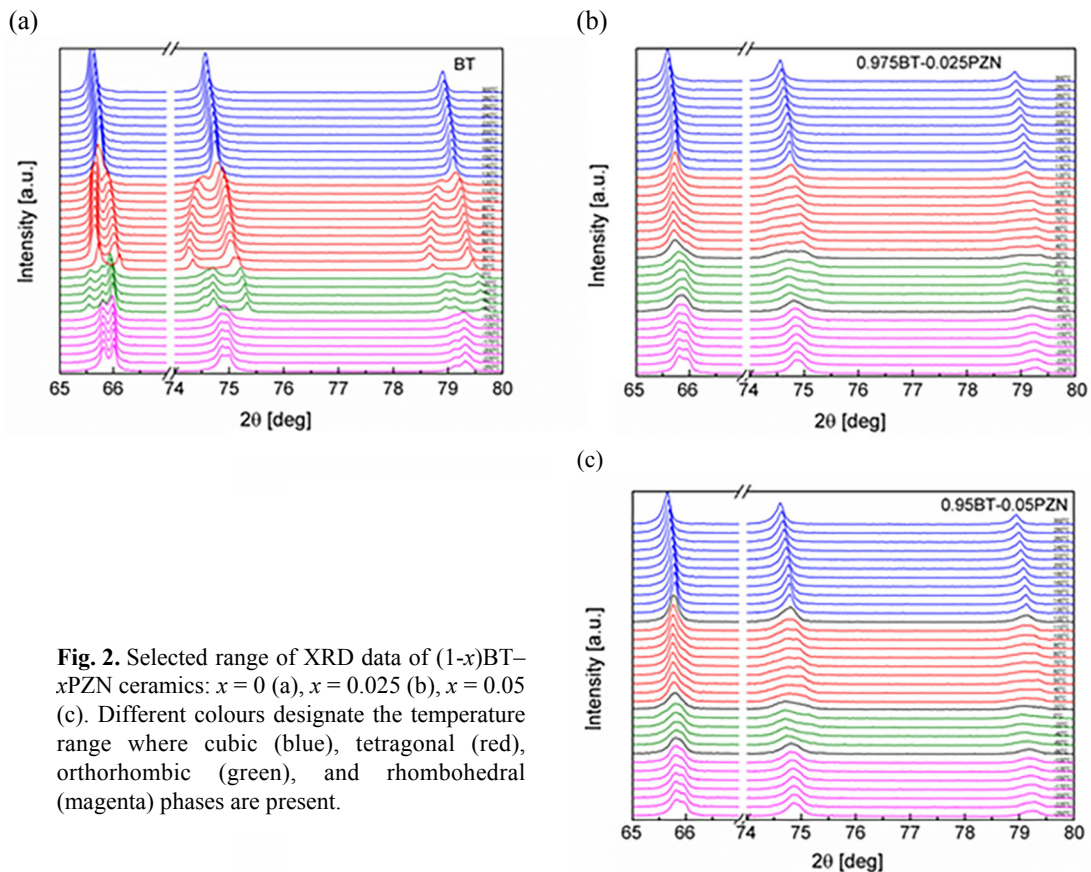

Fig. 2. Selected range of XRD data of (1-x)BT–xPZN ceramics: $x = 0$ (a), $x = 0.025$ (b), $x = 0.05$ (c). Different colours designate the temperature range where cubic (blue), tetragonal (red), orthorhombic (green), and rhombohedral (magenta) phases are present.

Fig. 3. Temperature dependence of the electric permittivity ε of (1-*x*)BT–*x*PZN ceramics on cooling.
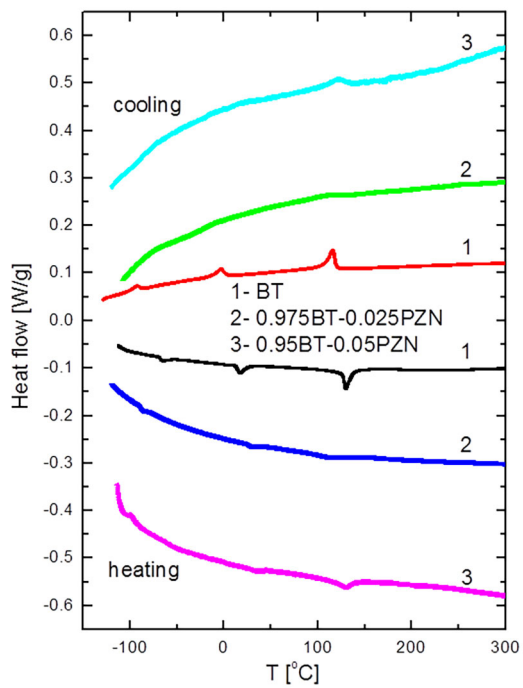
Fig. 4. Temperature evolution of the heat flow of (1-*x*)BT–*x*PZN ceramics.
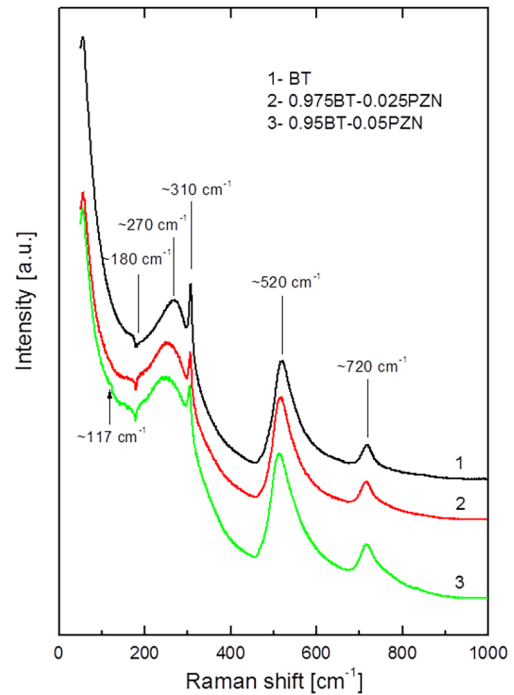

Fig. 5. Room temperature Raman spectra of (1-*x*)BT–*x*PZN ceramics.

However, detailed inspection of Fig. 5 shows some evolution of these spectra with a change of composition:
(1) First of all, some of the bands become broadened, which indicates that the crystal structure becomes more disordered. This is mainly related to the disorder created on A- and B-sites of BT after Pb and (Zn,Nb) substitution, respectively.
(2) In addition, some of the bands are shifted downwards from their frequencies in BT, which could be explained by the difference in the mass of Ba and Pb (Pb has a far bigger mass than Ba) and in the mass of Ti and (Zn,Nb) ((Zn,Nb) mass is bigger than the Ti mass). The bands at about 272 cm^{-1} and

at about 310 cm^{-1} decrease in intensity and move to the low-frequency range. Moreover, a new line appears at about 117 cm^{-1} for 0.95BT–0.05PZN (indicated by arrow), which may be evidence of a structural change associated with the A-site symmetry change. The high-frequency peaks are not detectably affected. The change of the 180 cm^{-1} mode and decrease in the intensity and broadening of the 310 cm^{-1} mode (both belong to the ferroelectric state for BT) with the increasing PZN content indicate that the ferroelectric properties are disturbed.

Figure 6 presents the temperature evolution of hysteresis loops of BT–PZN ceramics. As can be seen,
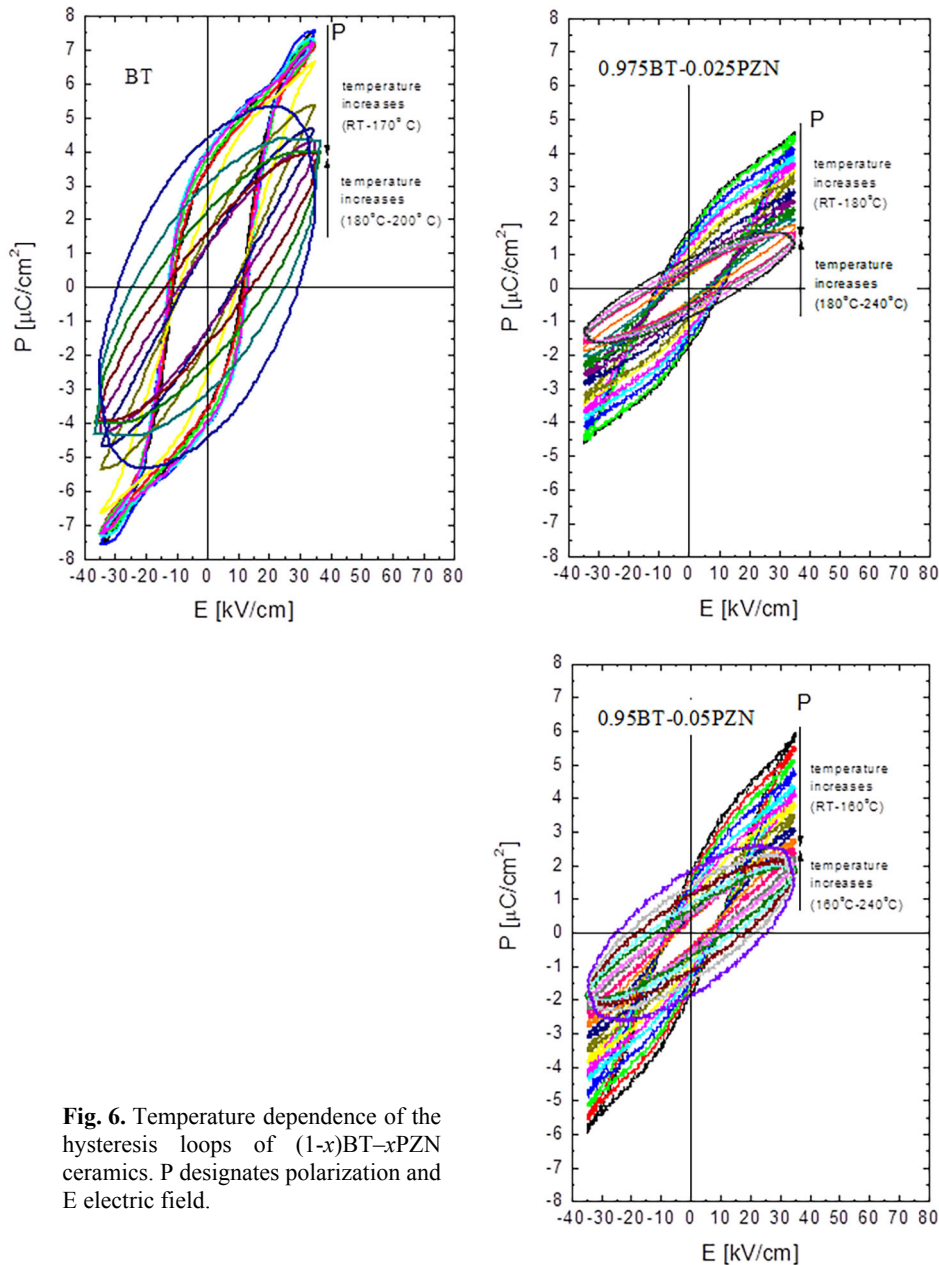
Fig. 6. Temperature dependence of the hysteresis loops of (1-*x*)BT–*x*PZN ceramics. P designates polarization and E electric field.

Table 1. Parameters of room-temperature hysteresis loops of $(1-x)$BT–xPZN ceramics: E_c – coercive field, P_m – maximal polarization, and P_r – remnant polarization

Composition	E_c [kV/cm]	P_m [μC/cm^2]	P_r [μC/cm^2]
$x = 0$	11.00	7.53	3.57
$x = 0.025$	10.76	4.64	1.73
$x = 0.05$	8.70	5.91	1.85

BT–PZN exhibits saturated hysteresis loops under the electric field of about 35 kV/cm. At a higher temperature these loops lose their pure ferroelectric character (at about 160, 180, and 190 °C for BT, 0.075BT–0.025PZN, and 0.95BT–0.05PZN, respectively), and these loops still exhibit hysterics behaviour even at higher temperatures, instead of being linear. This implies that polar regions exist in a nonpolar matrix in a wide temperature range above the temperature of phase transition for all ceramics (even for pure BT) in accordance with previous results [7–10]. Thermally increased electric conductivity at higher temperatures leads to a distortion of the hysteresis loops, which become nearly rounded and elliptical. The maximal and remnant polarization decrease after Pb and (Zn,Nb) ions substitution to BT (Table 1) is suggested from the Raman results. This can be mainly related to the increased degree of disorder of the material and the consequent disturbance of the long-range ferroelectric state of BT in accordance with the XRD and Raman results.

Due to the difference in the ion size between Ba^{2+} and Pb^{2+} and Ti^{4+} and (Zn,Nb)$^{4+}$, local elastic fields are expected. As B-site substitution is not isovalent, a charge imbalance can occur in BT. A cation vacancy can be created (as shown by Raman analysis) to compensate for this imbalance, and local electric fields will be generated. As a result, local electric fields (polar regions) will emerge, which can be responsible for the observed behaviour of the BT–PZN system.

4. CONCLUSIONS

Dense BT–PZN ceramics were fabricated via the SPS method. The samples exhibited a perovskite phase with no secondary impurity. Rietveld refinements of the XRD patterns indicated that the samples had single tetragonal symmetry at room temperature and possessed a sequence of phase transitions characteristic of pure BT.

The results are consistent with dielectric, DSC, and Raman data. Well-shaped hysteresis loops were observed for all samples. Temperature dependence of these loops indicated that polar regions existed in the temperature range above the ferroelectric–paraelectric phase transition.

REFERENCES

1. Moulson, A. J. and Herbert, J. M. *Electroceramics*. Chapman and Hall, London, 1990.
2. Hertling, G. H. Ferroelectric ceramics: history and technology. *J. Am. Cer. Soc.*, 1999, **82**, 797–918.
3. Nogas-Ćwikiel, E. and Suchanicz, J. Fabrication of 0.95BaTiO$_3$–0.05Pb(Mg$_{1/3}$Nb$_{2/3}$)O$_3$ ceramics by conventional solid state reaction method. *Arch. Metall. Mater.*, 2013, **58**, 1397–1399.
4. Suchanicz, J., Świerczek, K., Nogas-Ćwikiel, E., Konieczny, K., and Sitko, D. PbMg$_{1/3}$Nb$_{2/3}$O$_3$-doping effects on structural, thermal, Raman, dielectric and ferroelectric properties of BaTiO$_3$ ceramics. *J. Eur. Cer. Soc.*, 2015, **35**, 1777–1783.
5. Kreisel, J., Glazer, A. M., Jones, G. O., Thomas, P. A., Abello, P. A., and Lucazeau, G. An X-ray diffraction and Raman spectroscopy investigation of A-site substituted perovskite compounds: the (Na$_{1-x}$Ki$_x$)$_{0.5}$Bi$_{0.5}$TiO$_3$ ($0<x<1$) solid solution. *J. Phys. Condens. Matter.*, 2000, **12**, 3267–3280.
6. Farhi, R., El Marssi, M., Simon, A., and Ravez, J. A Raman and dielectric study of ferroelectric Ba(Ti$_{1-x}$Zr$_x$)O$_3$ceramics. *EPJ B*, 1999, **9**, 599–604.
7. Ziębińska, A., Rytz, D., Szot, K., Górny, M., and Roleder, K. Birefringence above T_c in single crystals of barium titanate. *J. Phys., Condens. Matter.*, 2008, **20**, 142202 (1–5).
8. Ko, J.-H., Kim, T. H., Roleder, K., Rytz, D., and Kojima, S. Precursor dynamics in the ferroelectric phase transition of barium titanate single crystals studied by Brillouin light scattering. *Phys. Rev. B.*, 2011, **84**, 094111 (1–6).
9. Bussmann-Holder, A., Beige, H., and Volkel, G. Precursor effects, broken local symmetry, and coexistence of order-disorder and displacive dynamics in perovskite ferroelectrics. *Phys. Rev. B.*, 2009, **79**, 184111 (1–6).
10. Zalar, B., Laguta, V. V., and Blinc, R. NMR evidence for the coexistence of order-disorder and displacive components in barium titanate. *Phys. Rev. Lett.*, 2003, **90**, 037601–037612.

Pb(Zn$_{1/3}$Nb$_{2/3}$)O$_3$ lisamise mõju BaTiO$_3$ keraamika struktuursetele, dielektrilistele, Ramani ja ferroelektrilistele omadustele

Jan Suchanicz, Halina Czternastek, Kamila Kluczewska, Piotr Czaja, Adrian Węgrzyn, Mariusz Sokolowski, Erazm Maria Dutkiewicz ja Jerzy Szczęsny

Uuriti, kuidas Pb(Zn$_{1/3}$Nb$_{2/3}$)O$_3$ (PZN) lisamine mõjutab BaTiO$_3$ (BT) omadusi süsteemis (1-x)BT–xPZN, kus $x = 0$, 0,025 ja 0,05. Röntgendifraktsioonanalüüs näitas, et saadud proovidel on tetragonaalse sümmeetriaga perovskiidi struktuur ja need läbivad puhta BT jaoks iseloomuliku faasiüleminekute jada. Mikrostruktuuri uuring näitas tihedat struktuuri, mis oli 95% ulatuses kooskõlas Archimedese meetodiga määratud suhtelise tihedusega. Dielektrilised mõõtmised näitasid, et pärast dopeerimist BT dielektriline läbitavuse maksimum laienes ja nihkus. Ramani spektrid on kõigi proovide puhul sarnased, mis on kooskõlas röntgendifraktsiooni andmetega. Tuvastati, et dopeerimine põhjustas ferroelektriliste omaduste halvenemist. Saadud tulemusi selgitatakse kristallstruktuuri ebakorrapära suurenemisega, mis tekitab lokaalse pinge- ja elektrivälja. Uuritud keraamikat peetakse heaks lähtepunktiks väikese plii-sisaldusega elektrooniliste materjalide loomisel.